Inorg. Chem. **2005**, *44*, 2297–2309

Photophysical, Spectroscopic, and Computational Studies of a Series of Re(I) Tricarbonyl Complexes Containing 2,6-Dimethylphenylisocyanide and 5- and 6-Derivatized Phenanthroline Ligands

John M. Villegas, Stanislav R. Stoyanov, Wei Huang, and D. Paul Rillema*

Department of Chemistry, Wichita State University, 1845 North Fairmount Street, Wichita, Kansas 67260-0051

Received August 31, 2004

The ligand 2,6-dimethylphenylisocyanide (CNx) forms six complexes of the formula $[Re(CO)_3(CNx)(L)]^+$, where L = 1,10-phenanthroline (**1**), 5-chloro-1,10-phenanthroline (**2**), 5-nitro-1,10-phenanthroline (**3**), 5-methyl-1,10-phenanthroline (**4**), 5,6-dimethyl-1,10-phenanthroline (**5**), and 1,10-phenanthrolinopyrrole (**6**). The lowest-energy absorption peaks of the complexes red-shift in the order **1** < **2** < **3** < **4** < **5** < **6**. The time-dependent density functional theory (TDDFT) and conductor-like polarizable continuum model (CPCM) computed singlet excited states in ethanol deviate by 1000 cm^{-1} or less from the experimental UV–vis peaks. The complexes undergo reversible reductions and irreversible oxidations. The electronic energy gap increases in the order **3** < **2** < **1** < **4** < **5** < **6**, which is the order of increasing electron-donating power of the phen substituents. The reduction potentials linearly correlate with the B3LYP calculated LUMO energies for **1**–**6**. The complexes emit at room temperature and at 77 K except **3**, which emits only at 77 K. The calculated ^{3}MLLCT energies are within 1100 cm^{-1} from the experimental emission energies at 77 K. The 77 K emission curve-fitting analysis results agree with the computational assignment of the emitting state as ^{3}MLLCT for **1**–**5** and ^{3}LC for **6**. The experimental 77 K emission energies and the calculated ^{3}MLLCT state energies increase in the order **6** < **5**, **3** < **2** < **4**, **1**. The 77 K emission lifetimes increase upon addition of substituents from 65 μs for **1** to 171 μs for **2**, to 230 μs for **4** and **5**, and to 322 μs for **3**. The emission quantum yields at room temperature in solution are 0.77, 0.78, 0.83, 0.56, and 0.11 for complexes **1**, **2**, **4**, **5**, and **6**, respectively.

Introduction

Rhenium(I) tricarbonyl complexes containing bidentate heterocyclic ligands have been a source of interest for several years,[1−22] largely due to their potential use in solar energy conversion.[3,23−26] These complexes are ideally suited for such use because they display intense luminescence in the visible region of the spectrum and have long emission lifetimes.[27]

* Author to whom correspondence should be addressed. E-mail: paul.rillema@wichita.edu.

(1) Wrighton, M.; Morse, D. L. *J. Am. Chem. Soc*. **1974**, *96*, 998.
(2) Giordano, P. J.; Wrighton, M. S. *J. Am. Chem. Soc*. **1979**, *101*, 2888.
(3) Wrighton, M. S.; Geoffroy, G. L. *Organometallic Photochemistry*; Academic Press: New York, 1979; Chapter 2.
(4) Lees, A. *Chem. Rev.* **1987**, *87*, 711.
(5) Giordano, P. J.; Fredericks, S. M.; Wrighton, M. S.; Morse, D. L. *J. Am. Chem. Soc*. **1978**, *100*, 2257.
(6) Fredericks, S. M.; Luong, J. C.; Wrighton, M. S. *J. Am. Chem. Soc*. **1979**, *101*, 7415.
(7) Smothers, W. K.; Wrighton, M. S. *J. Am. Chem. Soc*. **1983**, *105*, 1067.
(8) Vogler, A.; Kisslinger, J. *Inorg. Chim. Acta* **1986**, *115*, 193.
(9) Juris, A.; Campagna, S.; Bidd, I.; Lehn, J. M.; Zeissel, R. *Inorg. Chem*. **1988**, *27*, 4007.
(10) Van Wallendael, S.; Shaver, R. J.; Rillema, D. P.; Yoblinski, B. J.; Stathis, M.; Guarr, T. F. *Inorg. Chem*. **1990**, *29*, 1761.
(11) Sahai, R.; Rillema, D. P.; Shaver, R. J.; Van Wallendael, S.; Jackman, D. C.; Boldaji, M. *Inorg. Chem*. **1989**, *28*, 1022.
(12) Ruminski, R.; Cambron, R. T. *Inorg. Chem*. **1990**, *29*, 1574.
(13) Baiano, J. A.; Carlson, D. L.; Wolosh, G. M.; DeJesus, D. E.; Knowles, C. F.; Szabo, E. G.; Murphy, W. R., Jr. *Inorg. Chem*. **1990**, *29*, 2327.
(14) Tapolsky, G.; Duesing, R.; Meyer, T. J. *J. Phys. Chem*. **1989**, *93*, 2885.
(15) Tapolsky, G.; Duesing, R.; Meyer, T. J. *Inorg. Chem*. **1990**, *29*, 2285.
(16) Lin, R.; Guarr, T. F. *Inorg. Chim. Acta* **1990**, *167*, 149.
(17) Lin, R.; Guarr, T. F.; Duesing, R. *Inorg. Chem*. **1990**, *29*, 4169.
(18) Kalyasundaram, K. *J. Chem. Soc., Faraday Trans. 2* **1986**, *82*, 2401.
(19) Sacksteder, L.; Zipp, A. P.; Brown, E. A.; Streich, J.; Demas, J. N.; DeGraff, B. A. *Inorg. Chem*. **1990**, *29*, 4335.
(20) Leasure, R. M.; Sacksteder, L.; Nesselrodt, D.; Reitz, G. A.; Demas, J. N.; DeGraff, B. A. *Inorg. Chem*. **1991**, *30*, 3722.
(21) Hino, J. K.; Della Ciana, L.; Dressick, W. J.; Sullivan, B. P. *Inorg. Chem*. **1992**, *31*, 1072.
(22) Della Ciana, L.; Dressick, W. J.; Sandrini, D.; Maestri, M.; Ciano, M. *Inorg. Chem*. **1990**, *29*, 2792.
(23) Meyer, T. J. *Pure Appl. Chem*. **1986**, *58*, 1193.

10.1021/ic048786f CCC: $30.25
Published on Web 03/03/2005

Generally, Re(I) tricarbonyl complexes are MLCT emitters, having broad and structureless emission bands that are sensitive to changes in the nature of the environment.[1,2,4−7,20] Thus, variations in the structure of the non-carbonyl bidentate as well as the ancillary ligands produce considerable effects on luminescence energies, lifetimes, and quantum yields. Depending on the chromophoric bidentate ligand or the ancillary "spectator" ligand used, the photochemical and photophysical properties of the complex can be fine-tuned.

Density functional theory (DFT) is a very useful method for interpreting experimental results from electrochemistry and electronic spectroscopy. Linear relationships of $E_{1/2(ox)}$ versus the highest occupied molecular orbital (HOMO) energies and $E_{1/2(red)}$ versus the lowest unoccupied molecular orbital (LUMO) energies for a series of isoelectronic Ru(II) diimine complexes were reported from our laboratory.[28] DFT calculations on the singlet ground and lowest-lying triplet-states of a series of Re(I) tricarbonyl complexes were used by others for investigating excited-state geometries and electronic structures.[29,30] Time-dependent density functional theory (TDDFT) calculated MLCT states and UV−vis spectra correlations were also reported for Re(I) complexes containing the ligand azophenine.[30c]

The TDDFT method treats molecules in the gas phase and does not always give the right electronic transition energies in solution.[31,32] A model used with more success for molecules in solution combines the TDDFT method with the conductor-like polarizable continuum model (CPCM). For example, we reported a correlation between UV−vis absorption energies of $[Ru(bpy)_2(CNx)Cl]^+$ and singlet excited-state energies computed in a series of seven solvents of varied polarity using the TDDFT/CPCM model.[32b] According to other reports, the tandem use of TDDFT and CPCM has produced dramatic changes in the assignments and the energies of the singlet excited states for Ru(II) and Os(II) polypyridyl complexes.[33] It is the primary method used in our study.

We have experimentally and computationally investigated the effect of the 2,6-dimethylphenylisocyanide (CNx) ligand on the complexes $[Re(bpy)(CO)(CNx)_3]^+$, $[Re(CNx)_5Cl]$, and $[Re(CNx)_6]^+$.[34] The highest emission quantum yield (ϕ_{em}) and emission lifetime (τ_{em}) were observed for $[Re(CO)_3(bpy)(CNx)]^+$.[34b] Here, we extend the study by varying the substituents attached on the 5- and 6-positions of 1,10-phenantholine in the $[Re(CO)_3(CNx)(phen)]^+$ moiety. The phenanthroline ligand has an enhancing effect on the ϕ_{em} and τ_{em} of the system, allowing one to compare the effects of the substituents on the photophysical properties of the system.

Experimental Section

Materials. The ligand 2,4-dimethylphenylisocyanide was purchased from Fluka. The ligands 1,10-phenanthroline, 5-chloro-1-10-phenanthroline, 5-NO_2-1,10-phenanthroline, and 5-methyl-1,10-phenanthroline were purchased from GFS Chemicals. The 5,6-dimethyl-1,10-phenanthroline ligand was purchased from Aldrich. The 1,10-phenanthrolinopyrrole ligand (php) was prepared in our laboratory.[35] Optima grade methanol was purchased from Fischer Scientific, while acetonitrile was purchased from Sigma-Aldrich. AAPER Alcohol and Chemical Co. was the source of absolute ethanol. The $[Re(CO)_5Cl]$ was purchased from Aldrich. Ethanol and methanol were used in a 4:1 (v/v) mixture to prepare solutions for the emission, and emission lifetime studies. Elemental analyses were obtained from M-H-W Laboratories, Phoenix, AZ.

Instrumentation and Physical Measurements. UV−vis spectra were obtained using a Hewlett-Packard model 8452A diode array spectrophotometer. The IR spectra were acquired using Nicolet Avatar 360 FT-IR spectrophotometer. Proton NMR spectra were obtained using a Varian Mercury 300 FT-NMR spectrometer. An EG&G PAR model 263A potentiostat/galvanostat was used to obtain the cyclic voltammograms. The measurements were carried out in a typical H-cell using a platinum disk working electrode, a platinum wire counter electrode, and Ag/AgCl reference electrode in acetonitrile. The supporting electrolyte used was 0.1 M tetrabutylammonium hexafluorophosphate (TBAH). Ferrocene was added for reference.

The sample preparation for emission studies involved dissolving a small amount of sample (∼2 mg) in the appropriate solvent, and the absorbance of the solution was measured. The concentration of the solution for luminescence studies was altered to achieve an absorbance of about 0.10 at the energy of excitation. Such a concentration provides enough material for data acquisition but excludes self-quenching processes. A 3−4 mL aliquot of the solution was then placed in a 10 mm diameter Suprasil (Heraeus) nonfluorescent quartz tube equipped with a tip-off manifold. The sample was then freeze−pump−thaw degassed for at least three cycles (to approximately 75 milliTorr) removing any gases from the sample. The manifold was then closed, and the sample was allowed to equilibrate at room temperature. The solvent evaporation

(24) Caspar, J. V.; Sullivan, B. P.; Meyer, T. J. *Inorg. Chem.* **1984**, *23*, 2098.
(25) Kober, E. M.; Marshall, J. L.; Dressick, W. J.; Sullivan, B. P.; Meyer, T. J. *Inorg. Chem.* **1985**, *24*, 2755.
(26) Kober, E. M.; Sullivan, B. P.; Dressick, W. J.; Caspar, J. V.; Mayer, T. J. *J. Am. Chem. Soc.* **1980**, *102*, 1383.
(27) Luong, J. C.; Nadjo, L.; Wrighton, M. S. *J. Am. Chem. Soc.* **1978**, *100*, 5790.
(28) Stoyanov, S. R.; Villegas, J. M.; Rillema, D. P. *Inorg. Chem.* **2002**, *41*, 2941.
(29) (a) Dattelbaum, D. M.; Martin, R. L.; Schoonover, J. R.; Meyer, T. J. *J. Phys. Chem. A* **2004**, *108*, 3518−3526. (b) Dattelbaum, D. M.; Omberg, K. M.; Hay, J. P.; Gebhart, N. L.; Martin, R. L.; Schoonover, J. R.; Meyer, T. J. *J. Phys. Chem. A* **2004**, *108*, 3527−3536.
(30) (a) Yang, L.; Ren, A.-M.; Feng, J.-K.; Liu, X.-J.; Ma, Y.-G.; Zhang, M.; Liu, X.-D.; Shen, J.-C.; Zhang, H.-X. *J. Phys. Chem. A* **2004**, *108*, 6797−6808. (b) Dyer, J.; Blau, W. J.; Coates, C. G.; Creely, C. M.; Gavey, J. D.; George, M. W.; Grills, D. C.; Hudson, S.; Kelly, J. M.; Matousek, P.; McGarvey, J. J.; McMaster, J.; Parker, A. W.; Towrie, M.; Weinstein, J. A. *Photochem. Photobiol. Sci.* **2003**, *2*, 542−554. (c) Frantz, S.; Rall, J.; Hartenbach, I.; Schleid, T.; Zalis, S. Kaim, W. *Chem.-Eur. J.* **2004**, *10*, 149−154.
(31) (a) Monat, J. E.; Rodriguez, J. H.; McCusker, J. K. *J. Phys. Chem. A* **2002**, *106*, 7399. (b) Rodrigues, J. H.; Wheeler, D. E.; McCusker, J. K. *J. Am. Chem. Soc.* **1998**, *120*, 12051.
(32) (a) Stoyanov, S. R.; Villegas, J. M.; Rillema, D. P. *Inorg. Chem.* **2003**, *42*, 7852. (b) Stoyanov, S. R.; Villegas, J. M.; Rillema, D. P. *Inorg. Chem. Commun.* **2004**, *7*, 838−841. (c) Villegas, J. M.; Stoyanov, S. R.; Huang, W.; Lockyear, L. L.; Reibenspies, J.; Rillema, D. P. *Inorg. Chem.* **2004**, *43*, 6383−6396.
(33) Guillemoles, J.-F.; Barone, V.; Joubert, L.; Adamo, C. *J. Phys. Chem. A* **2002**, *106*, 11345.
(34) (a) Villegas, J. M.; Stoyanov, S. R.; Reibenspies, J.; Rillema, D. P. *Organometallics* **2005**, *24* (3), 395−404. (b) Stoyanov, S. R.; Villegas, J. M.; Cruz, A. J.; Lockyear, L. L.; Reibenspies, J.; Rillema, D. P. *J. Chem. Theory Comput.* **2005**, *1* (1), 95−106.
(35) Villegas, J. M.; Stoyanov, S. R.; Rillema, D. P. *Inorg. Chem.* **2002**, *41*, 6688.

was assumed to be negligible; therefore, the concentrations were assumed to remain constant throughout this procedure. The corrected emission spectra were collected using a Spex Tau3 fluorometer.

The emission quantum yields were then calculated using eq 1, where ϕ_x is the emission quantum yield of the sample and ϕ_{std} is the emission quantum yield for the standard $[Ru(bpy)_3]^{2+}$, A_{std} and A_x represent the absorbance after degassing the standard and the sample, respectively, while I_{std} and I_x are the integrals of the emission envelope of the standard and the sample, respectively.[36]

$$\phi_x = (A_{std}/A_x)(I_x/I_{std})\phi_{std} \quad (1)$$

The excited-state lifetimes were determined by exciting the sample at 355 nm using an OPOTEK optical parametric oscillator pumped by a frequency tripled Continuum Surlite Nd:YAG laser run at ~20 mJ/10 ns pulse. The oscilloscope control and data curve-fitting analysis were accomplished using the Origin 6.1 program by OriginLab Corp. The excited-state lifetime experiments were conducted as previously published.[35]

Preparation of *fac*-[Re(CO)$_3$(CNx)(L)](PF$_6$). The complexes were synthesized according to previously published procedures,[37,38] which were modified as follows: A 0.55 mmol sample of $[Re(CO)_5Cl]$ was added to an equimolar amount of the phenanthroline-based ligand in a 125 mL round-bottomed flask. Approximately 50 mL of absolute ethanol was added, and the mixture was refluxed for 2−4 h. A colored precipitate formed in the solution, which was cooled to room temperature and filtered. After drying in a vacuum oven for 3−5 h, about 0.20 mmol of the product was added to an equimolar amount of $AgCF_3SO_3$ in a 125 mL round-bottomed flask. Again, approximately 50 mL of absolute ethanol was added, and the mixture was refluxed for 4−6 h. The solution was cooled to room temperature, and the AgCl precipitate was removed by filtration. An equimolar amount of the CNx ligand dissolved in 10 mL of ethanol was added to the filtrate, and the solution was again refluxed for another 3−5 h. The solvent was reduced in volume (about 5−10 mL) under vacuum. A saturated NH_4PF_6 solution (15 mL) in water was then added, and the solution was diluted to 50 mL with water (or until precipitation was completed). The precipitate was collected by filtration, dried in a vacuum oven, and weighed.

(1) *fac*-[Re(CO)$_3$(CNx)(phen)](PF$_6$). Color: yellow. Yield: 97%. Anal. Calcd for $ReC_{24}H_{17}N_3O_3PF_6$: C, 39.67; H, 2.36; N, 5.78. Found: C, 39.49; H, 2.20; N, 5.63. (KBr pellet): 2170, 2037, 1937, 1632, 1605, 1521, 1431, 1227, 1151, 841, 779, 724, 634, 558, 507, 471 cm^{-1}. ^{1}H NMR (DMSO): δ ppm 1.72 (s, 6H), 7.06 (d, 2H, J = 7.5 Hz), 7.19 (dd, 1H, J = 0.9, 8.1 Hz), 8.18 (dd, 2H, J = 3.3, 5.1 Hz), 8.38 (s, 2H), 9.06 (dd, 2H, J = 1.2, 8.4 Hz), 9.57 (dd, 2H, J = 1.5, 5.1 Hz).

(2) *fac*-[Re(CO)$_3$(CNx)(5-Cl-phen)](PF$_6$). Color: light yellow. Yield: 81%. Anal. Calcd for $ReC_{24}H_{16}N_3O_3ClPF_6$ (containing 0.8 mol of SiO_2): C, 35.63; H, 2.12; N, 5.52. Found: C, 35.50; H, 2.18; N, 5.46. (KBr pellet): 2172, 2040, 1971, 1938, 1653, 1603, 1559, 1519, 1426, 1209, 972, 842, 727, 635, 610, 558 cm^{-1}. ^{1}H NMR (DMSO): δ ppm 1.78 (s, 6H), 7.07 (d, 2H, J = 7.8 Hz), 7.21 (dd, 1H, J = 1.2, 8.1 Hz), 8.19 (dd, 1H, J = 3.3, 5.1 Hz), 8.28 (dd, 1H, J = 3.3, 5.1 Hz), 8.72 (s, 1H), 8.98 (dd, 1H, J = 1.2, 8.4 Hz), 9.16 (dd, 1H, J = 1.2, 8.4 Hz), 9.57 (dd, 1H, J = 1.5, 5.1 Hz), 9.65 (dd, 1H, J = 0.9, 5.1 Hz).

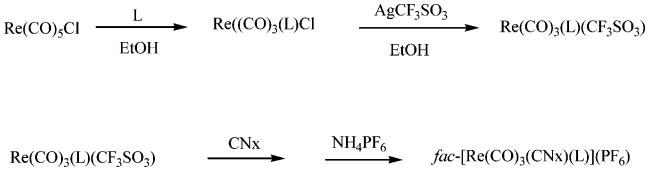

Figure 1. Schematic diagram of the synthesis of the complexes.

(3) *fac*-[Re(CO)$_3$(CNx)(5-NO$_2$-phen)](PF$_6$). Color: yellow. Yield: 80%. Anal. Calcd for $ReC_{24}H_{16}N_4O_5PF_6$: C, 37.36; H, 2.09; N, 7.26. Found: C, 37.50; H, 2.16; N, 7.22. (KBr pellet): 2174, 2041, 1973, 1939, 1684, 1653, 1541, 1521, 1473, 1457, 1345, 1159, 844, 756, 663, 635, 558, 420 cm^{-1}. ^{1}H NMR (DMSO): δ ppm 1.80 (s, 6H), 7.07 (d, 2H, J = 7.5 Hz), 7.20 (dd, 1H, J = 1.2, 8.1 Hz), 8.29 (m, 2H), 9.25 (dd, 1H, J = 1.2, 8.4 Hz), 9.34 (dd, 1H, J = 1.2, 8.7 Hz), 9.44 (s, 1H), 9.69 (dd, 2H, J = 1.2, 5.4 Hz).

(4) *fac*-[Re(CO)$_3$(CNx)(5-Me-phen)](PF$_6$). Color: light yellow. Yield: 80%. Anal. Calcd for $ReC_{25}H_{19}N_3O_3PF_6$: C, 40.54; H, 2.59; N, 5.67. Found: C, 40.30; H, 2.77; N, 5.57. (KBr pellet): 2171, 2037, 1968, 1937, 1653, 1630, 1559, 1522, 1429, 1389, 1159, 1032, 842, 728, 635, 611, 558, 478 cm^{-1}. ^{1}H NMR (DMSO): δ ppm 1.73 (s, 6H), 2.87 (s, 3H), 7.06 (d, 2H, J = 7.5 Hz), 7.20 (dd, 1H, J = 1.2, 8.4 Hz), 8.14 (m, 2H), 8.20 (s, 1H), 8.93 (dd, 1H, J = 1.5, 8.4 Hz), 9.09 (dd, 1H, J = 1.5, 8.4 Hz), 9.48 (dd, 1H, J = 1.5, 5.1 Hz), 9.57 (dd, 1H, J = 1.2, 5.1 Hz).

(5) *fac*-[Re(CO)$_3$(CNx)(5,6-Me$_2$-phen)](PF$_6$). Color: light yellow. Yield: 77%. Anal. Calcd for $ReC_{26}H_{21}N_3O_3PF_6$ (containing 0.5 mol of SiO_2): C, 39.80; H, 2.70; N, 5.36. Found: C, 39.86; H, 2.66; N, 5.54. (KBr pellet): 2170, 2037, 1968, 1935, 1653, 1614, 1602, 1475, 1432, 1174, 1034, 842, 727, 635, 558, 478 cm^{-1}. ^{1}H NMR (DMSO): δ ppm 1.75 (s, 6H), 2.83 (s, 6H), 7.07 (d, 2H, J = 7.5 Hz), 7.21 (dd, 1H, J = 1.2, 8.1 Hz), 8.16 (dd, 2H, J = 3.3, 5.1 Hz), 9.16 (dd, 2H, J = 1.5, 8.7 Hz), 9.51 (dd, 2H, J = 1.2, 5.1 Hz).

(6) *fac*-[Re(CO)$_3$(CNx)(php)](PF$_6$). Color: yellow. Yield: 90%. Anal. Calcd for $ReC_{26}H_{18}N_4O_3PF_6$: C, 40.79; H, 2.37; N, 7.32. Found: C, 41.00; H, 2.14; N, 7.15. (KBr pellet): 2169, 2035, 1966, 1934, 1602, 1524, 1472, 1441, 1381, 1281, 1252, 1160, 1102, 1072, 1030, 846, 779, 730, 637, 608, 558, 541, 478, 429 cm^{-1}. ^{1}H NMR (DMSO): δ ppm 1.80 (s, 6H), 7.07 (d, 2H, J = 7.5 Hz), 7.22 (dd, 1H, J = 1.2, 8.1 Hz), 8.27 (dd, 2H, J = 0.9, 6.5 Hz), 9.11 (s, 2H), 9.51 (dd, 2H, J = 0.9, 10.4 Hz), 9.81 (d, 2H, J = 10.4 Hz), 13.60 (s, 1H).

Results

Synthesis. The synthesis of the complexes was carried out according to the scheme presented in Figure 1. The $[Re(CO)_5Cl]$ was first reacted with the phenanthroline-based ligand (L) to form a neutral complex with the general formula $[Re(CO)_3(L)Cl]$. The product then was allowed to react with $AgCF_3SO_3$ removing the chloro ligand from the coordination sphere by precipitating AgCl and replacing it with $CF_3SO_3^-$. The CNx ligand then replaced $CF_3SO_3^-$ by reaction of $[Re(CO)_3(L)(CF_3SO_3)]$ with a slight excess of CNx added to the filtrate. After refluxing the solution for about 3 h and reducing the volume by rotary evaporation, the final product was precipitated by adding a saturated solution of NH_4PF_6 and diluting it with more water until precipitation was complete. The products were formed in relatively high yield.

(36) (a) Demas, J. N.; Crosby, G. A. *J. Phys. Chem.* **1971**, *75*, 991. (b) Cook, M. J.; Lewis, A. B.; McAuliffe, G. S. G.; Skarda, V.; Thomson, A. J.; Glasper, A. L.; Robbins, D. J. *J. Chem. Soc., Perkin Trans. 2* **1984**, 1293.
(37) Wallace, L.; Rillema, D. P. *Inorg. Chem.* **1993**, *32*, 3836−3843.
(38) Shaver, R. J.; Rillema, D. P. *Inorg. Chem.* **1992**, *31*, 4101.

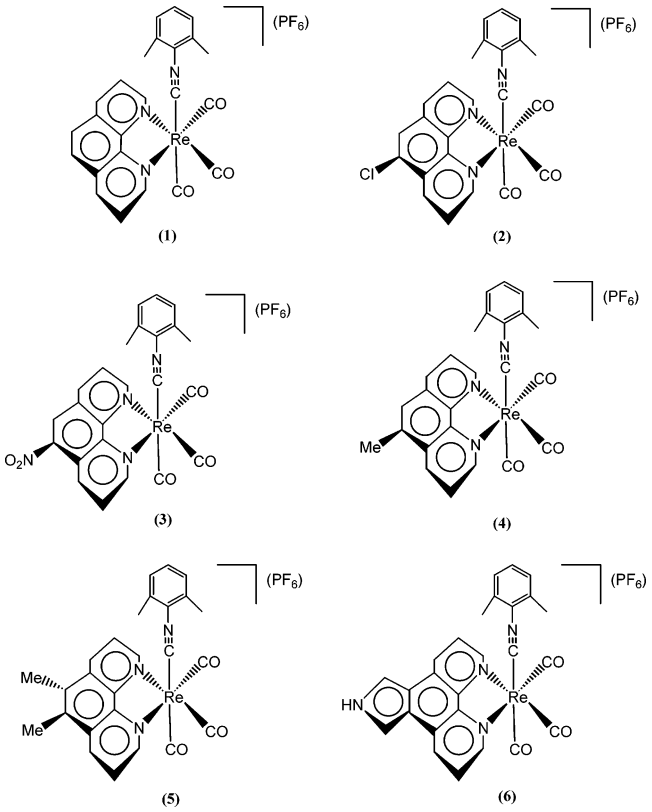

Figure 2. Structures of the complexes used in the study.

Figure 2 shows a schematic diagram of the Re(I) tricarbonyl isocyanide complexes with the phenanthroline-based ligands. As noted in this series, the complexes are *facial* and only the 5- and/or 6-positions of the parent phenanthroline ligand were modified by substituting the hydrogen atoms with electron-withdrawing or electron-donating groups.

Electronic Absorption Studies. The electronic absorption properties of the complexes were studied at room temperature using 4:1 (v/v) ethanol/methanol as solvent, and spectra are shown in Figure 3. The absorption coefficients of the transitions involved were determined from Beer's Law studies using at least five dilution points. The probable assignments of these bands were made on the basis of the computational assignment of the singlet excited states and the documented optical transitions of similar types of complexes.[1−3,27,39] The results are listed in Table 1.

The lowest energy transitions of the complexes were assigned as metal−ligand-to-ligand-charge transfer (MLLCT) for **1**−**5** and as a ligand-centered (LC) transition for **6**. Several $\pi \rightarrow \pi^*$ transitions were reported for the complexes at higher energies. It is important to note that because the MLLCT band occurs as a broad shoulder, the exact position of the band as well as the extinction coefficient were subject to error.

The MLLCT peak did not significantly shift from **1** for **2** and **3** as the electron-withdrawing groups Cl and NO_2 were attached in the 5-position of the parent phen ligand. The bands were located at 27 500 cm^{-1} for **1** and **2**. The MLLCT band of **3** was red-shifted by 500 cm^{-1} relative to **1**. When electron-donating methyl groups were attached in **4** and **5** positions, the MLLCT band was red-shifted to 26 900 cm^{-1} in **4** and 26 500 cm^{-1} in **5**. Upon extension of the phen aromatic system in **6**, the lowest energy peak was observed at 24 400 cm^{-1} and assigned as a LC state (vide infra).

Electrochemical Studies. The redox potentials of the complexes in the series were determined by cyclic voltammetry and are listed in Table 2. All complexes in the series showed irreversible oxidation waves in the range of 1.97−2.05 V.

The reduction potentials increased from −1.18 V for **1** to −1.08 for **2** and −0.53 V for **3** when the hydrogen atom in the 5-position of the parent phen ligand was replaced with an electron-withdrawing substituent. However, the potentials shifted in the opposite direction from −1.18 V for **1** to −1.24 V for **4**, to −1.26 V for **5** and to −1.51 V for **6** when the hydrogen atom(s) in 5 and/or 6 position of the parent phen ligand were replaced with electron-donating methyl group(s) in complexes **4** and **5** or with a pyrrole group in complex **6**.

Emission Properties and Excited-State Lifetimes. The emission properties and excited-state lifetimes (τ_{em}) of the complexes were determined both at room temperature and at 77 K in 4:1 (v/v) ethanol/methanol. The values of the emission lifetimes at room temperature and 77 K were determined by curve-fitting analysis. The data are listed in Table 3. Temperature-dependent studies of the emission lifetimes were not conducted because the complexes underwent photodecomposition upon continuous exposure to laser radiation.

The emission maxima of the complexes were shifted to higher energies at 77 K as compared to room temperature as shown in Figure 4. The 77 K emission maxima of complexes **2**−**6** were red-shifted relative to complex **1** regardless of the nature or the number of the substituents attached. The emission energies ranged from 21 800 cm^{-1} for **1** to 21 100 cm^{-1} for **2** and 20 400 cm^{-1} for **3**, or underwent a red-shift of 700 and 1400 cm^{-1}, respectively. Relative to **1**, the emission maxima red-shifted by 200 cm^{-1} when an electron-donating methyl group was attached in complex **4** and by 1100 cm^{-1} when a second methyl group was attached in complex **5**. The largest red shift of 1800 cm^{-1} was recorded for complex **6** relative to **1** when the conjugated pyrrole π-system was attached.

After converting the wavelength (abscissa) values to energy, the emission spectral data were fit to eq 2, where the summation was carried out over the two sets of six vibrational levels.[40]

$$I(E) = I_0 + A[\sum_{n1}\sum_{n2}[(E_0 - n_1\hbar\omega_1 - n_2\hbar\omega_2)/E_0]^4 (S_1^{n1}/n_1!)(S_2^{n2}/n_2!) \exp\{-4 \log 2[(E - E_0 + n_1\hbar\omega_1 + n_2\hbar\omega_2)/\upsilon_{1/2}]^2\}] \quad (2)$$

(39) Juris, A.; Belser, P.; Barigelletti, F.; von Zelewsky, A.; Balzani, V. *Inorg. Chem.* **1986**, *25*, 256.

(40) (a) Caspar, J. V. Ph.D. Thesis, University of North Carolina, Chapel Hill, NC, 1982. (b) Allen, G. H.; White, R. P.; Rillema, D. P.; Meyer, T. J. *J. Am. Chem. Soc.* **1984**, *106*, 2613.

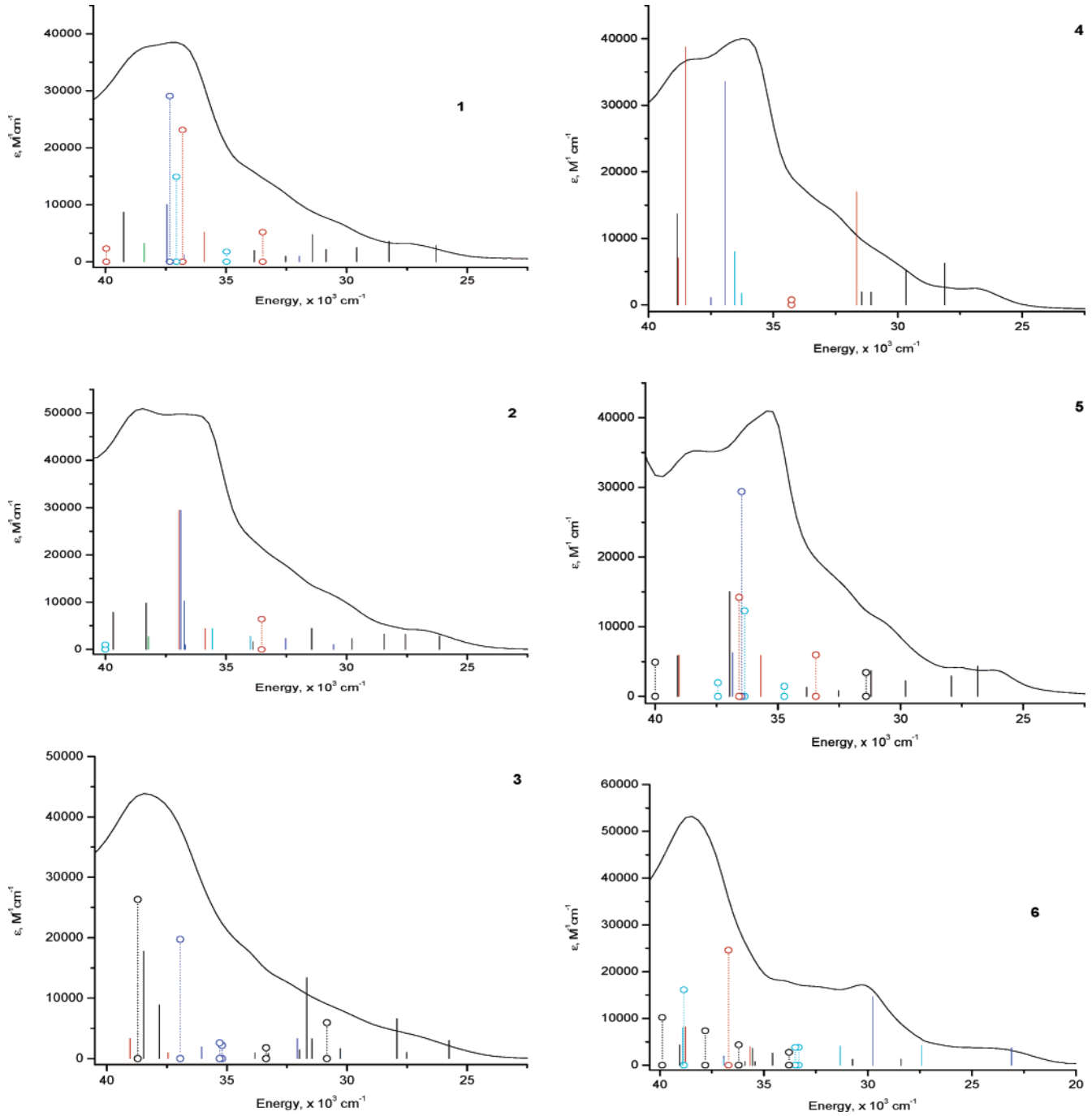

Figure 3. Experimental absorption spectra of **1**−**6** and calculated singlet excited states. The excited states are shown as vertical bars with height equal to the extinction coefficient.[31a] Black = MLLCT, green = LLCT, blue = $\pi \rightarrow \pi^*$, red = MCDCT, cyan = LCDCT (ligand → delocalized), and ○·····○ = mixed excited state.

The parameters were as follows: I_0 was equal to 0, A was the peak area, n_1, $n_2 = 0-5$, E_0 was the zero−zero energy, $\hbar\omega_1$ and $\hbar\omega_2$ represented the energies of the high and low vibrational frequency acceptor modes, S_1 and S_2 were the measures of the distortion in the high- and low-frequency acceptor modes,[41] and $\upsilon_{1/2}$ was the full-width at half-maximum of the zero−zero vibronic component in the emission spectra. The maximum intensity was adjusted to 1 for the curve-fitting analysis.

The results of the emission spectral curve-fitting at 77 K (Figure 4) are listed in Table 4. The values of the high-frequency modes at about 1400 cm^{-1} correspond to the phen ligand ring breathing modes. For complexes **1**−**5**, the low-frequency modes were attributed to metal−ligand vibrations. For complex **6**, curve-fitting analysis using one set of six vibrational levels produced more reasonable values than for a two-set curve-fitting analysis as was used for the others.

(41) The spatial distribution of the singly occupied orbitals in the excited state can be determined from the vibrational frequency acceptor modes. Example: for the MLCT state, the high-frequency acceptor mode would be the ligand ring breathing mode and the low-frequency acceptor mode would be related to the vibrations of metal−ligand bonds. The coefficients S_1 and S_2 are indicative of the relative contributions of the high and the low vibrational modes to the fine vibronic structure of the emission.

Table 1. Experimental[a] Electronic Transitions and Calculated[b] Singlet Excited States of Re(I) Complexes **1**−**6**

complex	E_{exp}, $\times 10^3$ cm^{-1} ϵ (M^{-1} cm^{-1})	E_{calc}, $\times 10^3$ cm^{-1}	assignment
1	27.5 (3300)	28.2	MLLCT
	33.3 (15 000)	33.5	MCDCT
	37.0 (39 700)	37.1	CDLCT
	38.5 (37 500)	38.4	LLCT
2	27.5 (4800)	27.6	MLLCT
	36.2 (49 600)	35.9	MCDCT
	38.5 (50 900)	38.3	MLLCT
3	27.0 (3500)	27.5	MLLCT
	38.5 (38 600)	38.5	MLLCT
	42.4 (36 900)		LC ($\pi\rightarrow\pi^*$)
4	26.9 (3000)	28.1	MLLCT
	36.2 (39 300)	36.3	LCDCT
	38.5 (36 000)	38.5	MCDCT
	42.7 (39 900)		LC ($\pi\rightarrow\pi^*$)
5	26.5 (3400)	26.9	MLLCT
	35.5 (40 600)	35.7	MCDCT
	38.5 (34 500)	39.1	MLLCT
	41.7 (43 100)		LC ($\pi\rightarrow\pi^*$)
6	24.4 (3700)	23.1	LC ($\pi\rightarrow\pi^*$)
	30.3 (17 600)	30.7	MLLCT
	38.5 (51 900)	38.8	MCDCT
	44.2 (49 300)		LC ($\pi\rightarrow\pi^*$)

[a] In 4:1 (v/v) ethanol:methanol. [b] In ethanol.

Table 2. Electrochemical Properties of the Complexes in CH_3CN at Room Temperature

complex	$E_{1/2(ox)}$, V[a]	$E_{1,2(red)}$, V[a] (L)
1	2.01[b]	−1.18
2	2.03[b]	−1.08
3	2.05[b]	−0.53
		−1.06
4	2.00[b]	−1.24
5	1.98[b]	−1.26
6	1.97[b]	−1.51

[a] Potential in volts vs SSCE (scan rate = 250 mV/s). [b] Irreversible oxidation wave.

Computational Section. The singlet ground-state geometries of complexes **1**−**6** were optimized in the gas phase using the B3LYP[42] functional of the Gaussian 03[43] program package. The Stuttgart−Dresden (SDD) ECP[44] was used for the Re core potentials. The {(8s7p6d)/[6s5p3d]}-GTO was applied for the valence shell of Re together with the all-electron 6-311G* basis set[45] for Cl, O, N, C, and H atoms. The optimized geometries of the complexes are listed in the Supporting Information Table S1.

Table 3. Calculated ^{3}MLLCT State Energies[a] and Emission Properties of the Complexes at 77 K and Room Temperature[b] (Energies in $\times 10^3$ cm^{-1}, s = shoulder)

complexes	E_{calc}	E_{exp} 77 K	E_{exp} room temp	τ_{em}, μs 77 K	τ_{em}, μs room temp	φ_{em}[c] room temp
1	22.6	21.8	19.7	65	8.6	0.77
		20.4				
		19.1				
		17.7 (s)				
2	22.2	21.1	19.1	171	1.5	0.78
		19.7				
		18.3				
		17.1 (s)				
3	20.9	20.4		322		
		19.0				
		17.8 (s)				
4	22.6	21.6	19.6	231	20.2	0.83
		20.2				
		18.8				
		17.5 (s)				
5	20.7	20.7	20.3	229	30.9	0.56
		19.3	19.3 (s)			
		18.0				
		16.6 (s)				
6	19.1	20.0	18.5	268	6.2	0.11
		18.6				
		17.3				
		16.0 (s)				

[a] In the gas phase. [b] In 4:1 (v/v) EtOH:MeOH. [c] Relative to $[Ru(bpy)^3]^{2+}$ (ref 35).

Nonequilibrium TDDFT[46]/CPCM[47] calculations were employed to produce a number of singlet excited states[48] of complexes **1**−**6** in ethanol based on the singlet ground-state geometry optimized in the gas phase.[49] The TDDFT/CPCM calculations are nonequilibrium calculations with respect to the polarization process between the solvent reaction field and the charge density of the electronic state indicated in the input. For singlet excited states, this is the singlet ground state.[50] The output contained information for the excited-state energies and oscillator strengths (*f*) and a list of the excitations that give rise to each excited state, the orbitals involved, as well as the wave function coefficients of the excitations. The singlet excited states of the six comp-

(42) (a) Becke, A. D. *J. Chem. Phys.* **1993**, *98*, 5648. (b) Lee, C.; Yang, W.; Parr, R. G. *Phys. Rev. B* **1988**, *37*, 785. (c) Vosko, S. H.; Wilk, L.; Nusair, M. *Can. J. Phys.* **1980**, *58*, 1200.

(43) Frisch, M. J.; Trucks, G. W.; Schlegel, H. B.; Scuseria, G. E.; Robb, M. A.; Cheeseman, J. R.; Montgomery, J. A., Jr.; Vreven, T.; Kudin, K. N.; Burant, J. C.; Millam, J. M.; Iyengar, S. S.; Tomasi, J.; Barone, V.; Mennucci, B.; Cossi, M.; Scalmani, G.; Rega, N.; Petersson, G. A.; Nakatsuji, H.; Hada, M.; Ehara, M.; Toyota, K.; Fukuda, R.; Hasegawa, J.; Ishida, M.; Nakajima, T.; Honda, Y.; Kitao, O.; Nakai, H.; Klene, M.; Li, X.; Knox, J. E.; Hratchian, H. P.; Cross, J. B.; Adamo, C.; Jaramillo, J.; Gomperts, R.; Stratmann, R. E.; Yazyev, O.; Austin, A. J.; Cammi, R.; Pomelli, C.; Ochterski, J. W.; Ayala, P. Y.; Morokuma, K.; Voth, G. A.; Salvador, P.; Dannenberg, J. J.; Zakrzewski, V. G.; Dapprich, S.; Daniels, A. D.; Strain, M. C.; Farkas, O.; Malick, D. K.; Rabuck, A. D.; Raghavachari, K.; Foresman, J. B.; Ortiz, J. V.; Cui, Q.; Baboul, A. G.; Clifford, S.; Cioslowski, J.; Stefanov, B. B.; Liu, G.; Liashenko, A.; Piskorz, P.; Komaromi, I.; Martin, R. L.; Fox, D. J.; Keith, T.; Al-Laham, M. A.; Peng, C. Y.; Nanayakkara, A.; Challacombe, M.; Gill, P. M. W.; Johnson, B.; Chen, W.; Wong, M. W.; Gonzalez, C.; Pople, J. A. *Gaussian 03*, revision B.03; Gaussian, Inc.; Pittsburgh, PA, 2003.

(44) Andrae, D.; Hauessermann, U.; Dolg, M.; Stoll, H.; Preuss, H. *Theor. Chim. Acta* **1990**, *77*, 123.

(45) (a) McLean, A. D.; Chandler, G. S. *J. Chem. Phys.* **1980**, *72*, 5639. (b) Krishnan, R.; Binkley, J. S.; Seeger, R.; Pople, J. A. *J. Chem. Phys.* **1980**, *72*, 650.

(46) (a) Stratmann, R. E.; Scuseria, G. E.; Frisch, M. J. *J. Chem. Phys.* **1998**, *109*, 8218. (b) Bauernschmitt, R.; Ahlrichs, R. *Chem. Phys. Lett.* **1996**, *256*, 454. (c) Casida, M. E.; Jamorski, C.; Casida, K. C.; Salahub, D. R. *J. Chem. Phys.* **1998**, *108*, 4439.

(47) (a) Cossi, M.; Barone, V. *J. Chem. Phys.* **2001**, *115*, 4708. (b) Barone, V.; Cossi, M. J. *Phys. Chem. A* **1998**, *102*, 1995. (c) Cossi, M.; Rega, N.; Scalmani, G.; Barone, V. *J. Comput. Chem.* **2003**, *24*, 669.

(48) The CPCM is designed to account for the bulk physical properties of the solvent. It does not account for specific solvent−solute interactions. The TDDFT is known to perform well for the computing of charge-transfer excited states between closely spaced moieties. The tandem use of CPCM and TDDFT is currently the most suitable computational approach for the treatment of the solvent effects to the transition metal complexes excited-state energies.

(49) Geometry optimization in solvents was not achieved. Partial optimizations (change in distance of less than 0.001 Å and change in angles of less than 0.01°) followed by TDDFT/CPCM calculation produced excited-state energies that were not in better agreement with the experimental excited-state energies than the excited-state energies based on the gas-phase optimized geometry.

(50) Frisch, Æ.; Frisch, M. J.; Trucks, G. W. *Gaussian 03 User's Reference, version 7.0*; Gaussian, Inc.: Carnegie, PA, 2003; p 206.

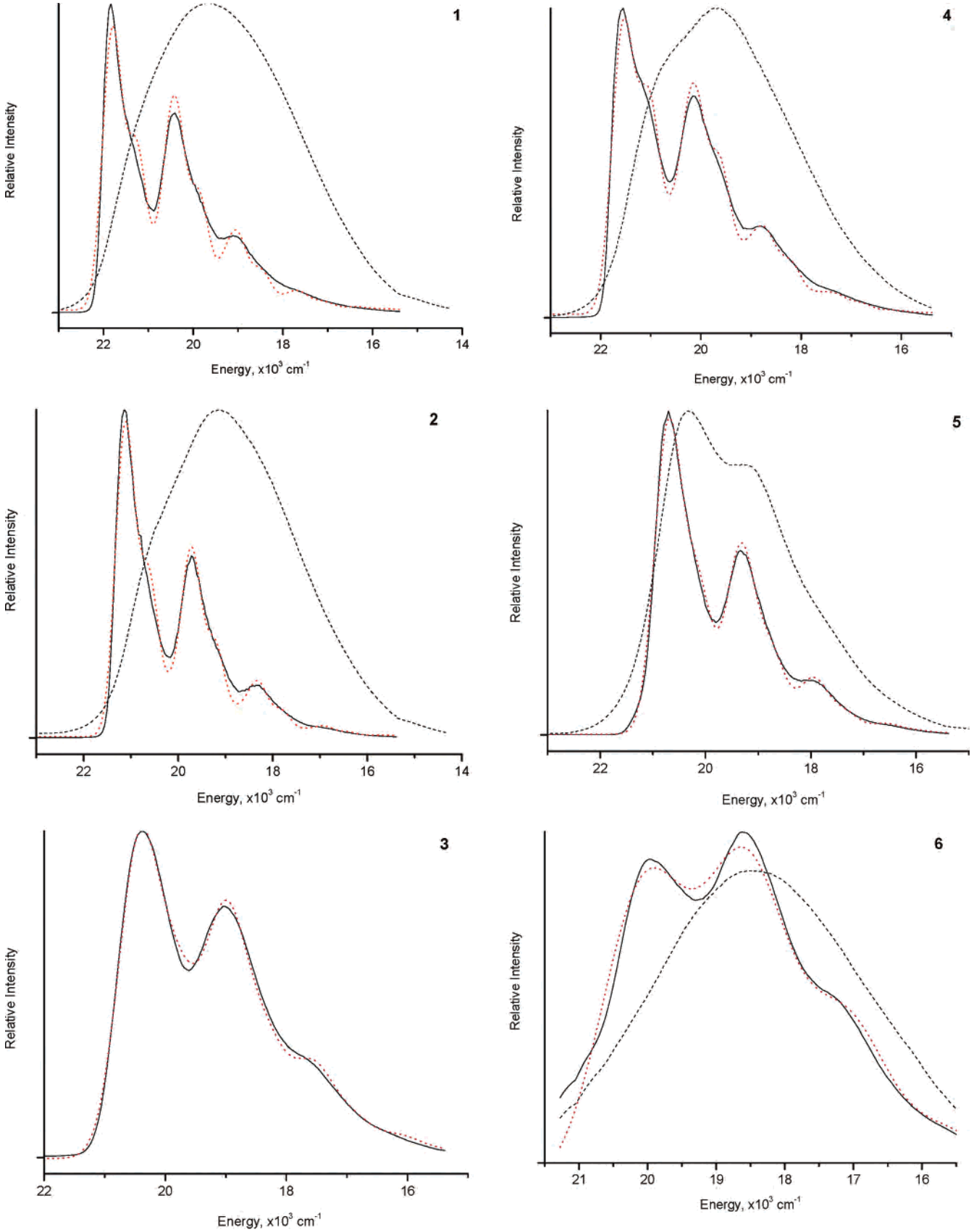

Figure 4. Emission spectra of the complexes at 77 K (−), curve-fitted (red ···), and at room temperature (− − −) in 4:1 (v/v) ethanol/methanol.

lexes are presented in Figure 3 as vertical bars with height equal to the extinction coefficient calculated from the oscillator strength.[31]

The lowest-lying triplet-state geometries of the six complexes were calculated using unrestricted B3LYP in the gas phase. The spin contamination from states of higher multi-

Table 4. Emission Spectral Curve-Fitting Parameters of Complexes **1**−**6** in 4:1 (v/v) EtOH/MeOH at 77 K[a]

parameter	**1**	**2**	**3**	**4**	**5**	**6**
E_{em}, cm^{-1}	21 800	21 100	20 400	21 600	20 700	20 000
E_0, cm^{-1}	21 800	21 120	20 440	21 550	20 710	20 000
$\hbar\omega_1$, cm^{-1}	1395	1401	1458	1414	1404	1460
S_1	0.89	0.75	0.88	0.88	0.72	1.40
$\hbar\omega_2$, cm^{-1}	545	505	661	525	570	
S_2	0.63	0.55	0.56	0.80	0.51	
$\upsilon_{1/2}$	510	480	800	520	610	1430
A	0.90	0.94	0.93	0.91	0.94	0.90

[a] Error limits are as follows: E_0, ±6.0 cm^{-1}, $\hbar\omega$, ±15 cm^{-1}, S, ±0.02, $\upsilon_{1/2}$, ±20 cm^{-1}, A, ±0.02.

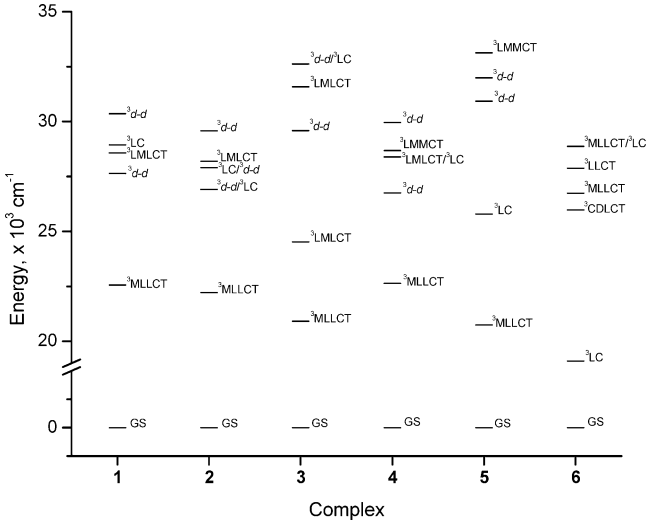

Figure 5. Triplet excited-state energy diagram for complexes **1**−**6**.

plicity was low. The value of $\langle S^2 \rangle$ was 2.017 for **1** and **2**, 2.009 for **3**, 2.015 for **4**, 2.041 for **5**, and 2.024 for **6**. The energies of the lowest-lying triplet states were higher than those of the corresponding ground states by 22 600 cm^{-1} for **1** and **4**, 22 200 cm^{-1} for **2**, 20 900 cm^{-1} for **3**, 20 700 cm^{-1} for **5**, and 19 100 cm^{-1} for **6** (Figure 5). The lowest-lying triplet states for complexes **1**−**5** were ^{3}MLLCT states, but for complex **6** it was a ^{3}LC state. These states featured single occupancy of the HOMO and the LUMO.

Four triplet excited states were computed in ethanol using the TDDFT/CPCM method based on the lowest-lying triplet-state geometries for each of the complexes and are listed in Table 5, even if the *f* values were low. The energies of these triplet excited states are given relative to the singlet ground state. The energies and the assignments of the lowest-lying triplet states and the four higher-lying triplet excited states from Table 5 are shown in Figure 5. These excited states were used for the interpretation of temperature-dependent emission properties of the complexes. The higher-lying triplet states were obtained via single electron vertical excitations from the lowest-lying ^{3}MLLCT states, and the excited-state energies reported were not the minima. The triplet excited states were calculated on the basis of the lowest-lying triplet state geometry because according to Kasha's rule this state would be the emitting state. Thus, the triplet excited states were determined on the basis of the most stable triplet geometry. Triplet excited states calculated on the basis of the singlet ground-state geometry are multiplicity forbidden ($f = 0$).

Table 5. Calculated Triplet Excited States of Complexes **1**−**6** in Ethanol Based on the Lowest-Lying Triplet State Geometry[a]

state	f	$\psi_o \rightarrow \psi_v$	type	E_{VER}
		Complex **1**		
1	0.01	H-2 → H (0.7)	Re_d, CO → Re_d, CNx	27.6
		H-1 → H (0.6)	Re_d → Re_d, CNx	
2	0.00	H-4 → H (1.0)	Phen, CNx → Re_d, CNx	28.6
3	0.01	L → L+1 (0.8)	LC $\pi \rightarrow \pi^*$	28.9
4	0.10	H-1 → H (0.7)	Re_d → Re_d, CNx	30.4
		H-2 → H (0.5)	Re_d, CO → Re_d, CNx	
		Complex **2**		
1	0.02	H-1 → H (0.7)	Re_d → Re_d, CNx	26.9
		L → L+1 (0.7)	LC $\pi \rightarrow \pi^*$	
2	0.00	L → L+1 (0.6)	LC $\pi \rightarrow \pi^*$	27.9
		H-2 → H (0.5)	Re_d, CO → Re_d, CNx	
3	0.00	H-4 → H (0.9)	5-Cl-phen → Re_d, CNx	28.2
4	0.10	H-1→ H (0.6)	Re_d → Re_d, CNx	29.6
		Complex **3**		
1	0.00	H-8 → H (0.8)	5-NO_2-phen → Re_d, CNx	24.5
2	0.00	H-1 → H (1.0)	Re_d → Re_d, CNx	29.6
3	0.00	H-2 → H (1.0)	CNx → Re_d, CNx	31.6
4	0.00	H-4 → H (0.8)	CNx, Re_d → Re_d, CNx	32.6
		Complex **4**		
1	0.00	H-1 → H (1.0)	Re_d, 5-Me-phen → Re_d, CNx	26.8
2	0.01	L → L+1 (0.6)	LC $\pi \rightarrow \pi^*$	28.4
		H-4 → H (0.6)	5-Me-phen, Re_d → Re_d, CNx	
		H-2 → H (0.5)	Re_d, CO → Re_d, CNx	
3	0.00	H-4 → H (0.8)	5-Me-phen, Re_d → Re_d, CNx	28.7
4	0.08	H-2 → H (0.7)	Re_d, CO → Re_d, CNx	30.0
		Complex **5**		
1	0.02	L → L+1 (1.0)	LC $\pi \rightarrow \pi^*$	25.8
2	0.02	H-1 → H (1.0)	Re_d, 5,6-Me_2-phen → Re_d, CNx	30.9
3	0.00	H-2 → H (1.0)	Re_d, CO → Re_d, CNx	32.0
4	0.00	H-3 → H (1.0)	5,6-Me_2-phen, Re_d → Re_d, CNx	33.1
		Complex **6**		
1	0.00	H-1 → H (0.8)	Del → php	26.0
2	0.02	H-2 → H (0.8)	Re_d, php → php	26.7
3	0.01	L → L+1 (1.0)	php → CNx, CO	27.9
4	0.00	H-3 → H (0.5)	Re_d, CO → php	28.9
		H-4 → H (0.5)	Re_d, php → php	
		L → L+2 (0.5)	LC $\pi \rightarrow \pi^*$	

[a] E_{VER} is the energy of the vertical transition in $\times 10^3$ cm^{-1}, *f* is the oscillator strength, and ψ_o and ψ_v are the occupied and the virtual orbitals that define the transition. The transition type is determined on the basis of the change in the spatial distribution from occupied to virtual orbital. The absolute value of the transition coefficient for each transition is given in parentheses. H = HOMO and L = LUMO. (See text for calculation details.)

Discussion

Molecular Orbitals. The 12-frontier molecular orbital energy diagram for complexes **1**−**6** in ethanol is shown in Figure 6. Schematic diagrams of the HOMOs and the LUMOs of complexes **1**−**6** are shown in Figure 7. The HOMOs of complexes **1**−**5** (Figure 7) contained 45% or higher Re_d character and 27% or higher CNx ligand character. The HOMOs−1 of complexes **1**, **2**, and **3** contained 61% or higher Re_d contributions. Additionally, there were 16% diimine ligand contributions for each of complexes **1** and **2** as well as 13% for complex **3**. The HOMOs−1 contained 43% or higher Re_d and 27% or higher diimine ligand contributions for complexes **4** and **5**. For complexes **1**, **2**, **4**, and **5**, the HOMOs−2 contained 66% or

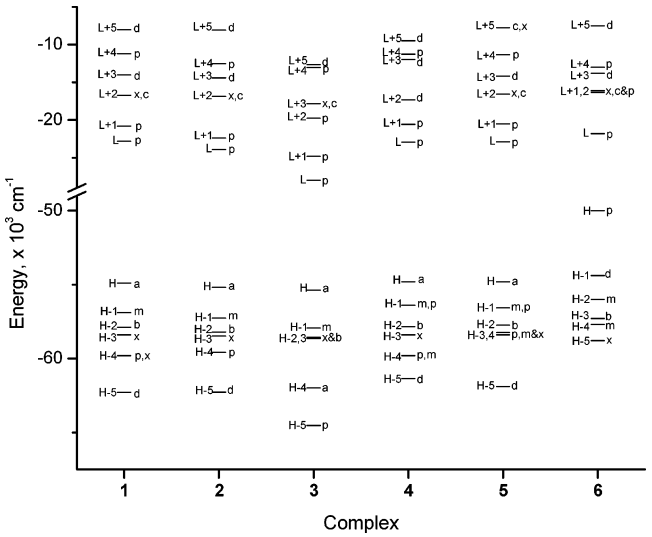

Figure 6. Molecular orbital energy diagram for six occupied (H) and six virtual (L) frontier orbitals of **1**−**6** in the singlet ground state in ethanol. a = Re_d, CNx, b = Re_d, CO, c = CO, d = delocalize, m = Re_d, p = phen-based ligand, and x = CNx. For example, orbitals H-3 and H-4 of complex **5** are assigned as p,m&x where H-3 is on the phen-based ligand (p) and Re_d (m) but H-4 is on the CNx ligand (x).

higher Re_d character and 20% or higher carbonyl character. The HOMO−2 of complex **3** contained 98% CNx ligand contribution. The character of the HOMOs and HOMOs−2 for complexes **1**, **2**, **4**, and **5** closely resembled that of the $[Re(CO)_3(bpy)(CNx)]^+$ complex.[34b] The HOMOs−1, however, contained significant diimine ligand contributions for complexes **1**−**5** that were not found in $[Re(CO)_3(bpy)(CNx)]^+$.[34b] For complex **6**, the HOMO contained ∼100% php ligand character, whereas HOMO−1 contained 42% Re_d, 24% CNx, and 21% php ligand contributions; thus HOMO−1 was assigned as complex-delocalized. The HOMO−2 contained 43% Re_d and 34% php ligand contributions. The ligand-centered nature of the HOMO of complex **6** (Figure 7) did not correlate with the metal-containing nature of the HOMOs of previously reported rhenium diimine tricarbonyl complexes.[29,34]

The LUMOs of complexes **1**−**6** (Figure 4) contained 81% or higher diimine ligand contribution like the LUMO of $[Re(CO)_3(bpy)(CNx)]^+$.[34b] According to Figure 7, the LUMO of complex **6** contained primarily contributions from the phen portion of the php ligand. The LUMOs+1 of complexes **1**−**5** contained 82% or higher diimine ligand contribution, different from $[Re(CO)_3(bpy)(CNx)]^+$ where the LUMO+1 contained mostly CNx and CO character.[34b] The LUMO+1 of complex **6** contained 49% CNx and 19% CO character and was assigned as CNx, CO. The LUMOs+2 of complexes **1**, **2**, and **5** contained CNx and CO character, while those of complexes **3** and **6** contained 5-NO_2-phen and php characters, respectively. The LUMO+2 of complex **4** contained 16% Re_p and Re_d as well as 21% carbonyl, 48% CNx, and 16% 5-Me-phen contributions; it was assigned as complex-delocalized. The percent molecular orbital contributions for complexes **1**−**6** are listed in the Supporting Information Table S2.

The HOMO−LUMO energy differences were 32 100 cm^{-1} for **1**, 31 300 cm^{-1} for **2**, 27 400 cm^{-1} for **3**, 31 900 cm^{-1} for **4**, 32 000 cm^{-1} for **5**, and 28 200 cm^{-1} for **6**. The HOMO−LUMO energy gaps for complexes **1**, **2**, **4**, and **5** were within 700 cm^{-1} of the 32 000 cm^{-1} value for $[Re(CO)_3(bpy)(CNx)]^+$.[34b]

Electrochemical Behavior. The redox potentials of importance in discussing the electrochemistry of the complexes in the series are those that are derived from the processes involving the HOMO and the LUMO.[37] The HOMOs of complexes **1**−**5** consist of dπ orbitals located on the metal center and CNx ligand π orbitals. The LUMOs are predominantly located on the π^* orbital of the phen-based ligand. The irreversible oxidations of **1**−**5** that involve the removal of an electron from the HOMO could be due to the 27% or higher CNx ligand contribution. The one-electron reduction, on the other hand, involves addition of an electron to the π^* orbital localized on the diimine moiety.[51−53]

The addition of an electron-withdrawing group to the phen moiety shifted the reduction potentials to higher values in the order **1** < **2** < **3**. As expected on the basis of the electrochemical behavior of nitro-organic compounds, complex **3**, which contains the NO_2-group attached to phenanthroline, was easily reduced at −0.53 V. However, according to the computational results (Figure 7), the LUMO is delocalized onto the 5-NO_2-phen ligand, indicating the whole unit is reduced, not just the nitro group. The electron-donating methyl groups, on the other hand, shifted the reduction potentials to lower values in the order **5** < **4** < **1**. The extended conjugation of the php ligand in **6** resulted in the lowest reduction potential and the highest electronic energy gap ($\Delta E_{1/2} = E_{1/2(ox)} - E_{1/2(red)}$). The oxidation potentials of **1**−**6** did not vary significantly. As a consequence, the electronic energy gap increased in the order **3** < **2** < **1** < **4** < **5** < **6**. The linear dependence ($R^2 = 0.97 \pm 0.10$) between the reduction potentials and the LUMO energies for complexes **1**−**6** is shown in Figure 8. The slope of -0.81 ± 0.07 was less than −2.32 reported for a series of 10 isoelectronic Ru(II) diimine complexes.[28] A linear correlation ($R^2 = 0.95 \pm 0.15$) of the ordinary Hammett substituent constants (σ_p) for **1**−**5** versus $E_{1/2(red)}$ had a slope of 0.72 ± 0.09 and an intercept of -1.14 ± 0.04.[54] This result was similar to the slope of 0.97 and the intercept of −1.16 reported for $[Re(CO)_3(Etpy)(bpy)]^+$ complexes ($R^2 = 0.98$).[21] Similarly, a linear plot ($R^2 = 0.91 \pm 0.16$) of E_{LUMO} versus σ_p for **1**−**5** had a slope of -0.63 ± 0.11 and an intercept of -2.91 ± 0.04.

Reversible oxidations of the pyridine (py) analogues of complexes **1** and **5**, $[Re(CO)_3(phen)(py)]^+$ and $[Re(CO)_3(5,6\text{-}Me_2\text{-}phen)(py)]^+$, occurred at 1.69 and 1.66 V, respectively.[37] Replacement of py with CNx results in an increase in the oxidation potential by approximately 0.32 V. The

(51) Sullivan, B. P.; Bolinger, C. M.; Conrad, D.; Vining, W. J.; Meyer, T. J. *J. Chem Soc., Chem. Commun.* **1985**, 1414.
(52) Abruna, H. D.; Breiks, A. I. *J. Electroanal. Chem. Interfacial Electrochem.* **1986**, *201*, 347.
(53) O'Toole, T. R.; Sullivan, B. P.; Bruce, M. R. M.; Margerum, L. D.; Murray, R. W.; Meyer, T. J. *J. Electroanal. Chem. Interfacial Electrochem.* **1989**, *259*, 217.
(54) Gordon, A. J.; Ford, R. A. *The Chemists Companion*; John Wiley & Sons: New York, 1972; pp 145−146.

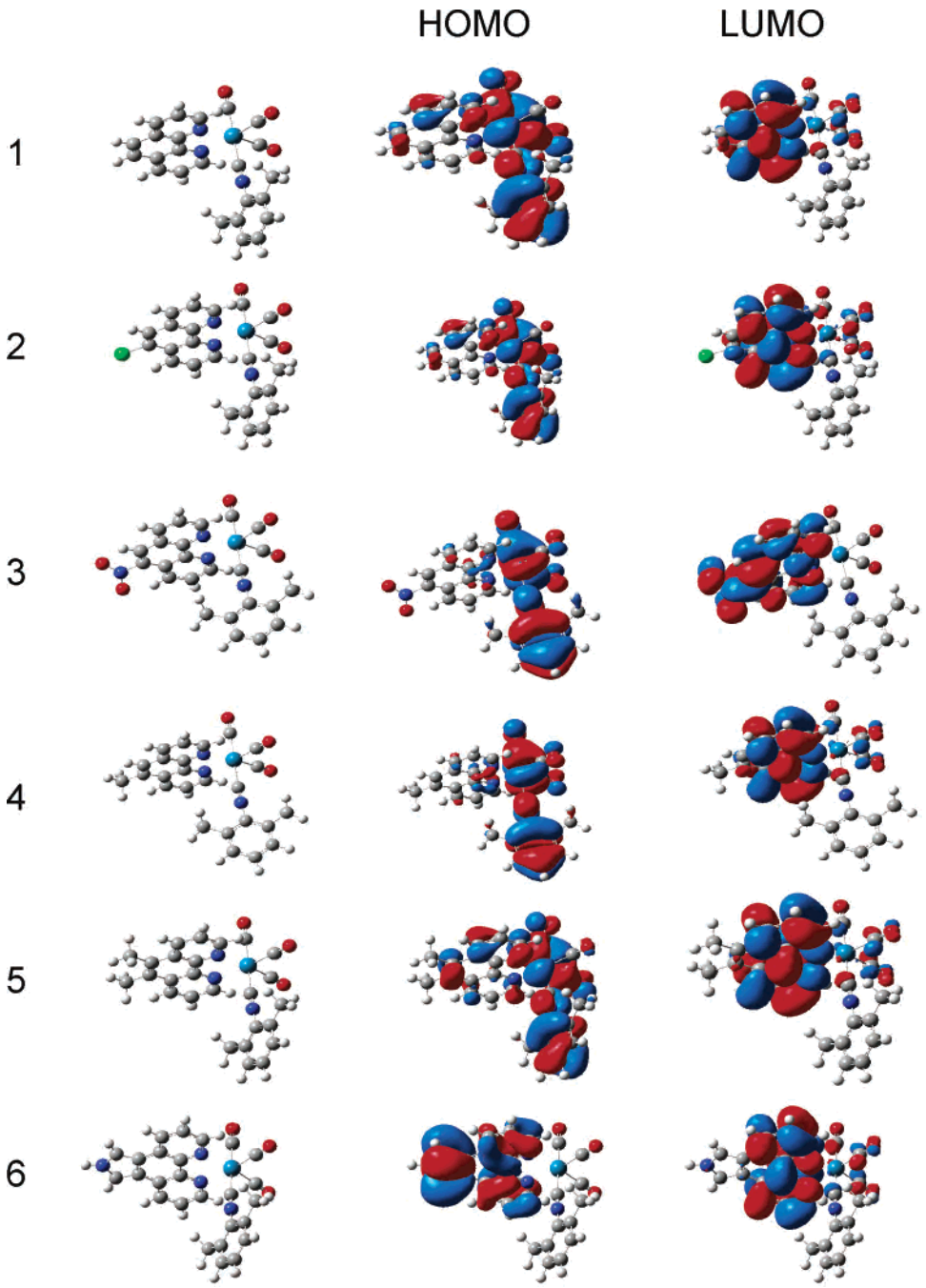

Figure 7. Schematic diagram of the HOMO and the LUMO of complexes **1**−**6**.

reduction potentials of these py analogues at −1.22 and −1.27 V[37] were slightly higher by 0.04 and 0.01 V as compared to the reduction potentials of **1** and **5**, respectively.

Singlet Excited States and Electronic Absorption Spectra. The singlet excited states of complexes **1**−**6** with $f > 0.01$ are shown in Figure 3 as vertical bars with height equal to the molar absorptivity coefficient (ϵ). The excited states expressed with the higher bars have higher contributions to the experimental peaks. Because calculated excited-state ϵ values have not correlated very well with the experimental values,[32b,c] we based our assignment of the experimental electronic transitions on the correlation of the calculated excited-state energies with the experimental peak energies. The bars are presented in colors that correspond to the type of the singlet excited state as follows: black = MLLCT, blue = $\pi \rightarrow \pi^*$, green = LLCT, red = MCDCT (metal to complex-delocalized charge transfer), and cyan = both LCDCT (ligand to complex-delocalized charge transfer) and CDLCT (complex-delocalized to ligand charge transfer). Mixed excited states are denoted with ○·····○.[55]

Excited-states 1 and 2 of complex **1** at 26 300 and 28 200 cm^{-1}, respectively, were associated with MLLCT transitions and correlated with the experimental UV−vis peak at 27 500 cm^{-1}. However, only the singlet excited-state 2 that is the closest in energy to the UV−vis peak is listed in Table 1. Excited-state 11 at 33 500 cm^{-1} was associated with a transition from the HOMO (Re_d and CNx) to the LUMO+3 (complex-delocalized) with a transition coefficient of 0.4 and

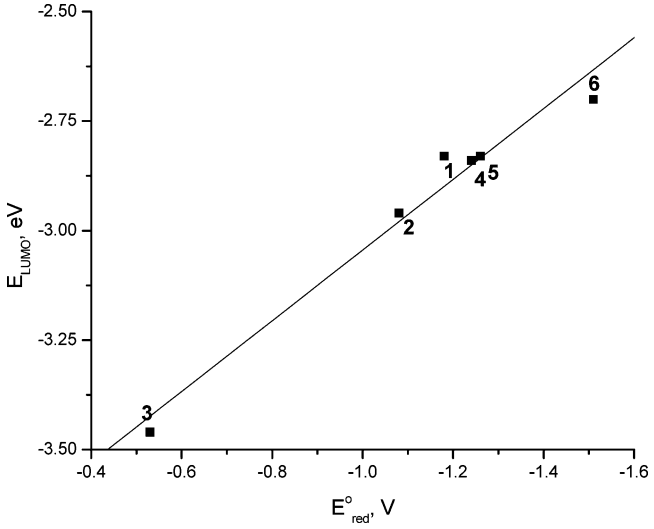

Figure 8. Linear dependence of $E_{1/2(red)}$ and the LUMO energies for complexes **1**−**6**.

was assigned as the MCDCT state. However, there were two more transitions, one from the HOMO−1 (Re_d) to LUMO+3 (complex-delocalized) assigned also as MCDCT and the other from HOMO−2 (Re_d and CO) to LUMO+2 (CNx, CO) assigned as MLLCT, each with transition coefficients of 0.3. Therefore, excited-state 11 is shown in Figure 3 as a mixed MCDCT state. This state was only 200 cm^{-1} higher in energy than the shoulder at 33 300 cm^{-1} in the experimental UV−vis spectrum. Excited-state 18 at 36 800 cm^{-1} was based on CDLCT and MCDCT transitions but was assigned as CDLCT on the basis of the higher transition coefficient. A similar approach was taken for excited-state 19 at 37 100 cm^{-1} Singlet excited-states 18 and 19 were correlated with the experimental peak at 37 000 cm^{-1}, but only state 19 that is 100 cm^{-1} blue-shifted relative to the experimental peak was listed in Table 1. The contribution of the phen $\pi\rightarrow\pi^*$ state 20 at 37 300 cm^{-1} to the latter experimental peak would be the highest because state 20 had the highest ϵ value of 29 100 M^{-1} cm^{-1} for complex **1**.

Excited-states 1 and 2 for complex **2** were of MLLCT type, and state 2 was 100 cm^{-1} blue-shifted relative to the experimental peak at 27 500 cm^{-1}. Several singlet excited states had energies near the experimental peak at 36 200 cm^{-1}. The MCDCT excited-state 17 at 35 900 cm^{-1} was 300 cm^{-1} red-shifted as compared to the latter experimental peak. Singlet excited-states 18, 19, and 20 assigned as 5-Cl-phen $\pi\rightarrow\pi^*$ states were in the range of 36 700−36 900 cm^{-1}. States 20 (ϵ = 29 400 M^{-1} cm^{-1}) and 21 (ϵ = 29 500 M^{-1} cm^{-1}) would have the highest contributions to the peak at 36 200 cm^{-1}.

(55) These assignments were made on the basis of the major contributing excitation. The singlet excited states had contributions from several excitations. For those presented with solid bars, there was a major contributing excitation (with a transition coefficient for the major excitation being higher than the transition coefficient of the other excitations by more than 0.2). For some singlet excited states, however, there was more than one contributing excitation with high transition coefficient. Singlet excited states that contained contributions from several excitations with transition coefficients that were within 0.2 of the major excitation transition coefficient are assigned as mixed singlet excited states and are presented with the symbol ○·····○.

The excited states below 30 000 cm^{-1} of complexes **3** and **4** were assigned as MLLCT. Four primarily LC $\pi\rightarrow\pi^*$ excited states were calculated in the range of 35 000−37 000 cm^{-1} for complex **3**. The highest contribution to the peak at 38 500 cm^{-1} was from the MLLCT state 28 (ϵ = 17 800 M^{-1} cm^{-1}) at the same energy. For complex **4**, the LCDCT states 16 and 17 at 36 300 and 36 500 cm^{-1} involve electronic transitions between ligand and complex-delocalized orbitals and are presented as cyan-colored bars. These states were blue-shifted by 100 and 300 cm^{-1}, respectively, relative to the experimental peak at 36 200 cm^{-1}. The highest contribution to the latter peak would be expected from the 5-Me-phen $\pi\rightarrow\pi^*$ state 18 (ϵ = 33 600 M^{-1} cm^{-1}). The MCDCT excited-state 22 (ϵ = 38 700 M^{-1} cm^{-1}) was at the same energy as the experimental peak at 38 500 cm^{-1}.

The excited states below 30 000 cm^{-1} for complex **5** were of MLLCT character. Singlet excite state 16 at 35 700 cm^{-1} based on a MCDCT transition was 200 cm^{-1} blue-shifted relative to the experimental peak at 35 500 cm^{-1}. The largest contribution to the latter peak can be attributed to exited state 18 (ϵ = 29 400 M^{-1} cm^{-1}) at 36 500 cm^{-1}, based on 5,6-Me_2-phen $\pi\rightarrow\pi^*$ and MCDCT transitions. Excited-states 23 and 24 at 39 000 and 39 100 cm^{-1} were assigned as MCDCT and MLLCT, respectively. The former was 500 cm^{-1} blue-shifted relative to the 38 500 cm^{-1} experimental peak.

In complex **6**, the excited-state 1 at 23 100 cm^{-1} was based on the HOMO → LUMO transition (Figure 7) and was assigned as a LC $\pi\rightarrow\pi^*$ state. If php is considered in terms of phen and pyrrole moieties, this state can be described as π(php)→π^*(phen) as shown in Figure 7. Excited-state 1 was 300 cm^{-1} red-shifted relative to the broad experimental UV−vis absorption peak at 24 400 cm^{-1}. The MLLCT excited-state 7 at 30 700 cm^{-1} was 400 cm^{-1} blue-shifted relative to the experimental peak at 30 300 cm^{-1}. Excited-state 22 at 36 700 cm^{-1} had the highest ϵ value of 24 600 M^{-1} cm^{-1}, and it was highly mixed. For state 22, the highest transition coefficient of 0.4 was from an MCDCT transition, but there were two more MLLCT transitions with coefficients of 0.3 and 0.2.

The experimental UV−vis peak at 38 500 cm^{-1} that appeared in the spectra of complexes **1**−**6** was assigned as LLCT for complex **1**, MLLCT for complexes **2**, **3**, and **5**, but as MCDCT for complexes **4** and **6**. The results from simulating Gaussian line shapes from the singlet excited states by integration following a procedure previously reported[31a] (not shown) did not correlate well with the UV−vis spectrum curvature. The use of the TDDFT/CPCM method is known to produce optical energies in good agreement with the experimental absorption spectra.[32c] However, the ϵ values produced from this method are found to deviate from the experiment.[32b] The singlet excited states are listed in the Supporting Information Table S3.

Triplet Excited States. Five low-lying triplet excited states of complexes **1**−**6** calculated relative to the ground state are presented in Figure 5. The lowest-lying triplet excited states of complexes **1**−**5** were ^{3}MLLCT states, but for complex **6** a ^{3}LC state was found. This computational assignment is supported by the results of the 77 K emission curve-fitting

analysis for **1**−**6**. For complexes **1**−**5**, the high and the low acceptor modes were related to ligand and metal−ligand vibrations, respectively. For complex **6**, only the high acceptor modes related to ligand vibrations were identified (vide supra). The emitting state for **6** can be described as π(php)→π*(phen). This assignment is analogous to the one reported for *fac*-[Re(CO)$_3$(dppz)(py)]$^+$, where dppz = dipyrido[3,2-a:2′,3′-c]phenazine.[30b] If we consider dppz in terms of phen and phenazine moieties, the emitting state was assigned as π (dppz) → π* (phenazine) based on picosecond and nanosecond visible, IR, and Raman spectroscopic studies supported by TDDFT calculations.[30b] Both the calculated ^{3}MLLCT and the experimental emission energies at 77 K decrease in the order **1** > **2** > **3** when electron-withdrawing substituents were added to the phen ligand. The calculated ^{3}MLLCT energies were higher than the experimental emission energies at 77 K by 800, 1100, 500, and 1000 cm^{-1} for complexes **1**, **2**, **3**, and **4**, respectively. The calculated ^{3}MLLCT and the experimental 77 K emission energies were the same for complex **5**. For complex **6**, the calculated ^{3}LC energy was lower than the experimental 77 K emission energy by 900 cm^{-1}.

Four low-lying triplet excited states calculated on the basis of the ^{3}MLLCT geometry are listed in Table 5. Triplet excited-state 1 (f = 0.01) of complex **1** (Table 5) was based on two ^{3}d−d excitations with transition coefficients of 0.7 and 0.6, respectively. The triplet excited-state 1 of complex **2** was a ^{3}d−d, ^{3}LC state, while for **3** it was a ^{3}LMLCT state. The triplet excited-state 1 (f = 0.00) of complex **4** was based on a Re$_d$, 5-Me-phen → Re$_d$, CNx transition and was assigned as a ^{3}MLLCT state. Excited-state 1 (f = 0.02) of complex **5** was of 5,6-Me$_2$-phen π→π* character. For complex **6**, excited-state 1 (f = 0.00) was associated with a transition between orbitals that contained complex-delocalized and php ligand contributions. It was assigned as a CDLCT state. Excited-state 1 of complex **3** was 3600 cm^{-1} higher in energy than the emitting ^{3}MLLCT state. This was the smallest energy difference between the emitting and the next higher triplet excited state, as compared to 5000 cm^{-1} for **1**, 4500 cm^{-1} for **2**, 4200 cm^{-1} for **4**, 5100 cm^{-1} for **5**, and 6900 cm^{-1} for **6**.

Triplet excited-state 2 (f = 0.00) of complex **1** located at 27 600 cm^{-1} was based on a phen, CNx → Re$_d$, CNx transition with a coefficient of 1.0 and was assigned as a ^{3}LMLCT state. Triplet excited-state 2 (f = 0.00) of complex **2** located at 17 900 cm^{-1} was a ^{3}d−d, ^{3}LC state similar to excited-state 1 of the same complex. Excited-state 2 (f = 0.01) of complex **4** was based on three transitions: ^{3}LC, ^{3}LMLCT, and ^{3}d−d with transition coefficients of 0.6, 0.6, and 0.5, respectively, and was assigned as a ^{3}LMLCT, ^{3}d−d state. Excited-state 2 of **5** was similar to state 1 of complex **4**. Excited-state 2 (f = 0.02) at 26 700 cm^{-1} of complex **6** was a ^{3}MLLCT state.

The TDDFT calculations for the triplet excited states presented in Figure 5 were performed relative to the ^{3}MLLCT states and did not account for spin−orbit coupling. For third-row transition metal complexes, the treatment with spin−orbit coupling could lower the predicted triplet-state energies through interactions with higher lying singlet and triplet states by 1700−2500 cm^{-1}.[56] The triplet excited-states 1 of complex **3** would then be thermally more accessible as compared to the excited-states 1 of the other five complexes, thus providing nonradiative relaxation pathways for **3**. Because the energy differences between the states given in Table 5 are for vertical transitions, the actual thermal activation energies could be lower.

Emission Properties and Excited-State Lifetimes. The emission spectra of the complexes are shown in Figure 4. Selected emission properties are listed in Table 3. The complexes exhibit broad emission spectra at room temperature, a typical behavior for ^{3}MLCT emitters.[37] Except for **3**, the complexes were emissive at room temperature; however, all complexes were highly emissive at 77 K.

The room-temperature emission peaks of the series showed a red-shift from 19 700 cm^{-1} for **1** to 19 100 cm^{-1} for **2** when the electron-withdrawing Cl was attached in the 5-position of the parent ligand. This shift in the emission peak is consistent with the decrease in the emission lifetime from 8.6 μs in complex **1** to 1.5 μs in **2** in accord with the energy gap law. The emission peak of complex **4** was red-shifted by 100 cm^{-1} relative to **1** when the electron-donating methyl group was attached. A more observable change was evident in **5**, when two methyl groups were added to the parent phen ligand. The emission peak of **5** was blue-shifted from 19 700 cm^{-1} for complex **1** to 20 300 cm^{-1}. The increase of the emission energy of **5** relative to **4** was accompanied by an increase of τ_{em} in agreement with the energy gap law. The room-temperature emission lifetimes in the series increased proportionally to the number of electron-donating methyl groups attached in the 5- and 6-positions of the parent ligand from 8.6 μs for **1** to 20.2 and 30.9 μs for complexes **4** and **5**, respectively. Increasing of the conjugation of the phen ligand in **6** resulted in a red-shift of the emission peak (18 500 cm^{-1}) and a decrease in τ_{em} (6.2 μs). Generally, the room-temperature emission lifetimes decreased as electron-withdrawing substituents were attached and increased when electron-donating groups were attached.

By definition, the decay rate constant, k, is related to the sum of the radiative and nonradiative decay rate, k_r and k_{nr}, respectively, ($k = k_r + k_{nr}$). Thus, the decrease in the emission lifetime of **1** as compared to **4** could be attributed to the decrease in the k_r term. In complex **6**, the increase of the conjugated system size from the parent phen ligand to php increased the nonradiative decay rate term, resulting in the decrease of the emission lifetime.

The emitting ^{3}MLCT state energy is essentially temperature dependent, as reported elsewhere.[34b,37] This dependency becomes more evident at low temperature when the emission maxima of the complexes in the series are shifted to higher energies. As a consequence of this shift, the emission spectra become structured typical for ^{3}LC emission. This could be due to the fact that at 77 K the ^{3}MLCT state shifts to a much

(56) Makedonas, C.; Mitsopoulou, C. A.; Lahoz, F. J.; Balana, A. I. *Inorg. Chem.* **2003**, *42*, 8853−8865.

higher energy than the ^{3}LC state, suggesting that under these conditions, the emission would most likely occur from a state that has a substantial ligand-centered character. The increase of the ^{3}LC character of emitting ^{3}MLCT states due to mixing of bpy $\pi\rightarrow\pi^*$ character into the MLCT state has been reported for *fac*-[Re(CO)$_3$(bpy)(4-ethylpyridine)]$^+$ based on B3LYP calculations.[29a] Emissions arising from ^{3}LC states are relatively insensitive to solvent and temperature effects, as these transitions involve minimal redistribution of electron density with respect to the solvent dielectric field.[37]

The 77 K emission lifetimes showed that when electron-withdrawing groups were attached, the emission lifetimes increased from 65 μs for **1** to 171 and 322 μs for **2** and **3**, respectively. The τ_{em} also increased to $\sim$230 μs when electron-donating methyl groups were attached in complexes **4** and **5**. The emissions lifetime of complex **6** increased to 268 μs.

The room-temperature emission lifetimes for the complexes were not directly related with their emission quantum yields (ϕ_{em}). All complexes except **3** had higher ϕ_{em} than the 0.089 value of standard complex [Ru(bpy)$_3$]Cl$_2$ (Table 3) under the same experimental conditions. Complexes **1** and **2** had quantum yields of 0.77 and 0.78, respectively. Complex **4** had a ϕ_{em} of 0.83, which decreased to 0.56 when the second methyl group was added in complex **5**. Complex **6** featured the lowest ϕ_{em} value of 0.11.

The emission maxima of [Re(CO)$_3$(phen)(py)]$^+$ and [Re(CO)$_3$(5,6-Me$_2$-phen)(py)]$^+$ were located at 20 100 and 16 400 cm^{-1} at 77 K in the same solvent.[37] Substitution of the CNx ligand for py[37] in complexes **1** and **5** caused a 1700 and 4300 cm^{-1} blue-shift for **1** and **5**, respectively, relative to their py analogues (at 77 K in the same solvent). This shift was accompanied by an increase of the 77 K emission lifetimes from 11.7 and 23 μs for the py analogues[37] to 65 and 229 μs for complexes **1** and **5**, respectively, in accord with the energy gap law.

Conclusions

A series of six complexes with the general formula [Re(CO)$_3$(CNx)(L)](PF$_6$), where L is a phenanthroline-based ligand with varying substituents in the 5- and 6-positions, was synthesized and investigated using spectroscopic and computational methods. The correlated results revealed the following: (1) The lowest energy transitions and the corresponding singlet excited states were MLLCT for complexes **1**−**5** and LC for complex **6**. (2) The electrochemical studies revealed that the irreversible ReII/I oxidation and reversible diimine ligand reduction potentials increased when electron-withdrawing groups (in **2** and **3**) were attached to the parent phenanthroline ligand and decreased when electron-donating groups were attached (in **4**, **5**, and **6**). (3) $E_{1/2(red)}$ was linearly dependent with E_{LUMO} and the Hammett constant σ_p. (4) E_{LUMO} and the Hammett constant σ_p were linearly related. (5) The complexes were highly emissive both at room temperature and at 77 K except **3** that was emissive only at 77 K. (6) The computational assignment of the emitting states as ^{3}MLLCT for **1**−**5** and ^{3}LC [π(php)$\rightarrow\pi^*$(phen)] for **6** was supported by the emission curve-fitting analysis results. (7) The room-temperature lifetimes decreased as electron-withdrawing substituents were attached and increased when electron-withdrawing groups were attached. (8) The 77 K lifetimes increased in the order **1** < **2** < **4**, **5** < **6** < **3**. (9) The quantum yields for the complexes were significantly higher than the standard, [Ru(bpy)$_3$]$^{2+}$, making the complexes potentially very good candidates for bimolecular excited-state electron-transfer reactions in solar energy conversion.

Acknowledgment. We thank the support of the National Science Foundation under Grant No. EIA-0216178 and Grant No. EPS-0236913, matching support from the State of Kansas and the Wichita State University High Performance Computing Center, the Wichita State University Office of Research Administration, the Department of Energy, and Parker Fellowships (J.M.V. and S.R.S.).

Supporting Information Available: The optimized geometries (Table S1), the percent orbital contributions (Table S2), and the calculated singlet excited-state energies of the six complexes (Table S3). This material is available free of charge via the Internet at http://pubs.acs.org.

IC048786F